Beta Rhythms (15–20 Hz) Generated by Nonreciprocal Communication in Hippocampus

Andrea Bibbig, Steven Middleton, Claudia Racca, Martin J. Gillies, Helen Garner, Fiona E. N. LeBeau, Ceri H. Davies and Miles A. Whittington

J Neurophysiol 97:2812-2823, 2007. First published 7 February 2007;
doi: 10.1152/jn.01105.2006

J Neurophysiol 97: 2812–2823, 2007.
First published February 7, 2007; doi:10.1152/jn.01105.2006.

Beta Rhythms (15–20 Hz) Generated by Nonreciprocal Communication in Hippocampus

Andrea Bibbig,[1] Steven Middleton,[2] Claudia Racca,[2] Martin J. Gillies,[2] Helen Garner,[2] Fiona E. N. LeBeau,[2] Ceri H. Davies,[3] and Miles A. Whittington[2]

[1]*Department of Physiology and Pharmacology, State University of New York Health Sciences Center, Brooklyn, New York;* [2]*School of Neurology, Neurobiology and Psychiatry, University of Newcastle, Newcastle; and* [3]*Psychiatry Centre of Excellence for Drug Discovery, GlaxoSmithKline Pharmaceuticals, Harlow, United Kingdom*

Submitted 16 October 2006; accepted in final form 28 January 2007

Bibbig A, Middleton S, Racca C, Gillies MJ, Garner H, LeBeau FE, Davies CH, Whittington MA. Beta rhythms (15–20 Hz) generated by nonreciprocal communication in hippocampus. *J Neurophysiol* 97: 2812–2823, 2007. First published February 7, 2007; doi:10.1152/jn.01105.2006. Generation of gamma rhythms in reciprocally connected areas of cortex produces synchronous neuronal firing, although little is known about the consequences of gamma rhythms when generated in nonreciprocally connected regions. This nonreciprocity exists in hippocampus, where gamma rhythms are generated in area CA3 in vitro and in vivo and nonreciprocally projected to area CA1 by the Schaffer collateral pathway. Here we demonstrate how this CA3 gamma rhythm generates two different patterns of local CA1 oscillation dependent on the degree of output from area CA1. *1*) In conditions where activity projected to area CA1 produces only very low principal cell recruitment the local population rhythm mimics the gamma rhythm projected from CA3. This activity is generated predominantly by recruitment of CA1 basket cells in a manner dependent on phasic, feedforward excitation of this interneuron subclass. Interneurons in stratum oriens, not receiving CA3 feedforward input, fired at theta frequencies. *2*) In the presence of serotonin CA1 principal cell recruitment was appreciably enhanced, resulting in dual activation of CA1 basket cells through both feedforward and feedback excitations. Feedback excitation to CA1 stratum oriens interneurons was also enhanced. The resulting change in interneuron network dynamics generated a beta-frequency CA1 rhythm (as a near-subharmonic of the gamma rhythm projected from CA3). These findings demonstrate that in nonreciprocally connected networks, the frequency of population rhythms in target areas serves to code for degree of principal cell recruitment by afferent input.

INTRODUCTION

Gamma rhythms in neocortex are generated in response to sensory input. They facilitate synchronous activity between both local and distal brain regions, with this synchrony closely associated with object recognition and short-term memory (Miltner et al. 1999; Rodriguez et al. 1999). The mechanism of synchrony associated with gamma rhythms was previously shown to depend on reciprocal synaptic connectivity between active neuronal networks (Traub et al. 1998). Reciprocal connectivity is widespread within the neocortex as a whole and also locally within subregions of nonneocortical structures such as hippocampus. However, no such reciprocal connections exist between areas CA3 and CA1 of hippocampus, begging the question: What role do gamma rhythms play, if any, in controlling the temporal pattern of CA1 outputs?

Rhythmic activity at gamma frequencies represents one of the primary working modes of the hippocampal formation. In vivo, gamma rhythms (30–80 Hz) are seen in dentate gyrus local field potentials where they appear to be projected from the entorhinal cortex (Chrobak et al. 2000). In the hippocampus proper, gamma rhythms are generated in area CA3 (Csicsvari et al. 2003; Fisahn et al. 1998) and unit activity in subpopulations of neurons (termed cell assemblies) occurred synchronously at gamma frequencies (Harris et al. 2003). However, during active exploration CA1 principal neuron activity is phased by theta-frequency rhythms, with mean firing rates in the beta band (15–20 Hz) (Huxter et al. 2003).

Hippocampal gamma rhythms are generated by the synchronous output of fast-spiking interneurons providing a phasic membrane potential change in principal cells at gamma frequencies (Fisahn et al. 1998; Whittington et al. 1995). Such activity occurs during periods of tonic excitation of interneurons or when interneurons are activated phasically by compound excitatory synaptic potentials from networks of gap-junctionally connected principal cells (Traub et al. 2000). The interneurons involved provide mainly perisomatically targeted trains of inhibitory postsynaptic potentials to pyramidal cells (Gillies et al. 2002; Mann et al. 2005) and consist predominantly of basket cells (Gloveli et al. 2005b; Hajos et al. 2004). In area CA1 these interneurons receive inputs from both feedforward pathways from area CA3 and feedback pathways from local CA1 pyramids (Sik et al. 1995). In contrast, horizontal CA1 interneurons, in particular oriens-lacunosum moleculare cells, receive predominantly local CA1 input (Ali and Thomson 1998; Blasco-Ibanez and Freund 1995) and do not fire at gamma frequencies. Instead they provide theta-frequency inhibition to distal dendrites of principal cells (Gillies et al. 2002; Gloveli et al. 2005a; Maccaferri and McBain 1996), even when receiving the same gamma-frequency network drive that produces a gamma-frequency output in basket cells (Whittington and Traub 2003).

In vitro hippocampal studies demonstrated a link between gamma oscillations and beta oscillations associated with enhancement of recurrent excitatory synaptic potentials in reciprocally connected networks within area CA1 (Whittington et al. 1997). These studies revealed that interneuron-mediated

Address for reprint requests and other correspondence: M. A. Whittington, School of Neurology, Neurobiology and Psychiatry, The Medical School, University of Newcastle, Newcastle NE2 4HH, UK (E-mail: m.a.whittington@ncl.ac.uk).

The costs of publication of this article were defrayed in part by the payment of page charges. The article must therefore be hereby marked "*advertisement*" in accordance with 18 U.S.C. Section 1734 solely to indicate this fact.

gamma-frequency oscillations persisted during the population beta oscillation, with principal cell spiking occurring only on every second or third period of this underlying gamma oscillation in a manner dependent on principal cell AHP amplitude and duration (termed *missed-beat beta*; Traub et al. 1999). This pattern of missed beats of an underlying gamma rhythm could also be generated by enhanced output from perisomatic targeting interneurons in a synaptic plasticity-dependent manner in computer simulations of hippocampal networks (Bibbig et al. 2002).

This particular pattern of principal cell recruitment by interneurons (involving missed beats of an underlying gamma rhythm) was shown to have a number of properties relevant to formation of cell assemblies in the temporal domain. First, beta-frequency oscillations of the missed-beat type are able to establish synchrony in discrete, active brain regions over greater distances than gamma rhythms alone (Kopell et al. 2000; von Stein et al. 1999). Second, different degrees of excitatory drive between two active, oscillating regions generate beta rhythms, with the principal cells in the two regions being recruited on alternate underlying gamma periods, resulting in two temporally separate principal cell assemblies (Olufsen et al. 2003).

These previous studies relied on generation of gamma rhythms directly within CA1 (a highly reciprocally connected region). We therefore sought to establish whether transitions from gamma to beta rhythms in area CA1 could occur when the system was driven in a more physiologically relevant manner by nonreciprocal inputs from the CA3 gamma-generating circuit. Changes in frequency of oscillating networks are well established in central pattern generating circuits (CPGs) in response to neuromodulation, particularly by 5-hydroxytryptamine (5-HT; Zhong et al. 1989). The hippocampus receives serotoninergic inputs from raphe neurons, with discharges temporally coordinated with hippocampal rhythms (Kocsis et al. 2006). We therefore used 5-HT, which increases CA1 pyramidal cell excitability as defined by spike rates for a given membrane potential (Colino and Halliwell 1987), to investigate the frequency component of any relationship between CA3 gamma rhythms and CA1 network-response states.

METHODS

Slice methods

Transverse hippocampal slices (450 μm) were prepared from adult Sprague–Dawley rats, anesthetized with inhaled isoflurane, immediately followed by an intramuscular (im) injection of ketamine ($\geq$100 mg kg^{-1}) and xylazine ($\geq$10 mg kg^{-1}). Animals were intracardically perfused with about 50 ml of modified artificial cerebrospinal fluid (ACSF), composed of (in mM): sucrose (252), KCl (3), NaH_2PO_4 (1.25), $NaHCO_3$ (24), $MgSO_4$ (2), $CaCl_2$ (2), and glucose (10). All salts were obtained from BDH (Poole, UK). The brain was removed and submerged in cold (4–5°C) ACSF during dissection. Horizontal slices were cut and then transferred to either a holding chamber or directly to a recording chamber. Here, they were maintained at 34°C at the interface between ACSF [composition (in mM): NaCl (126), KCl (3), NaH_2PO_4 (1.25), $NaHCO_3$ (24), $MgSO_4$ (2), $CaCl_2$ (2), and glucose (10)] and warm, moist carbogen gas (95% O_2-5% CO_2).

Drugs

All drugs, bath applied at known concentrations [DHPG, (*S*)-3,5-dihydroxyphenylglycine, 20–100 μM; NBQX, 2,3-dioxo-6-nitro-1,2,3,4-tetrehydrobenzo[*f*]quinoxaline-7-sulfonamide, 20 μM], were obtained from Tocris Cookson (Bristol, UK); 5-hydroxytryptamine (5-HT, 20 μM) was obtained from Sigma (Poole, UK).

Recording, data acquisition, and analysis

Extracellular recording electrodes were pulled from borosilicate glass (Harvard Apparatus, Kent, UK) filled with ACSF and had resistances in the range of 2–5 MΩ. Peak frequency and power values were obtained from power spectra generated with Fourier analysis in the Axograph software package (Axon Instruments). All values are given as means ± SE if the data sets were normally distributed; otherwise, data are presented as medians (interquartile range). Power spectra were constructed off-line from digitized data (digitization frequency: 10 kHz) using a 60-s epoch of recorded activity. Intracellular recordings from CA1 pyramidal cells and interneurons (nine "vertical" cells with dendritic arbors passing through the CA1 strata: eight basket cells, one bistratified cell; ten "horizontal" cells with dendritic arbors in stratum oriens: five oriens lacunosum moleculare interneurons, five oriens interneurons) were obtained with KCH_3SO_4-filled electrodes (resistance: 70–130 MΩ). During recording cells were filled with biocytin for post hoc reconstruction. The temporal profiles of both excitatory and inhibitory postsynaptic potentials (EPSPs and IPSPs, respectively) were taken by off-line averaging of 50 consecutive synaptic periods of activity (temporally aligned to the peak membrane potential change in each period) in each slice. EPSPs/IPSPs were automatically detected off-line using the event-detection routine in Axograph (Axon Instruments). Data are presented as grand averages pooled from five slices. Spike-frequency histograms were generated using Axograph software. Normally distributed data were compared using a standard paired *t*-test. Nonnormally distributed data were compared using a standard rank-sum (Mann–Whitney) test. Phase differences between CA3 and CA1 fields were calculated using a windowed cross-correlation function (200 ms) shifted at 100-ms intervals across the data set. Average phase difference was quantified as the temporal shift of the central peak in the cross-correlograms (resolution: 1 ms) and plotted against time.

Simulation methods

GENERAL NETWORK STRUCTURE. The computer program used for the present study was adapted from a program used to study persistent gamma oscillations in area CA3 of the hippocampal slice (Traub et al. 2000). Briefly, we constructed a network model of hippocampal area CA1 consisting of the following components: *1*) 3,072 pyramidal cells, each of them modeled as multicompartmental neurons with 64 somatodendritic and 10 axonal compartments; these pyramidal cells were organized in a 96 × 32 array; and *2*) 384 interneurons (46 somatodendritic, five axonal compartments) organized in a 96 × 4 array and consisting of the following classes: 288 interneurons with dendritic trees oriented vertically across all laminae (vertical interneurons)—96 basket cells, 96 axo-axonic cells, 96 bistratified cells—and 96 horizontal interneurons (olm cells) with a dendritic tree confined to stratum oriens.

STRUCTURE OF PYRAMIDAL CELLS AND INTERNEURONS. Pyramidal cell models contained the following active conductances: an inactivating Na^+ conductance g_{Na}, a persistent Na^+ conductance $g_{NA(P)}$, $g_{K(DR)}$ (delayed rectifier), a high-voltage–activated noninactivating g_{Ca}, a voltage- and Ca^{2+}-dependent fast K^+ conductance $g_{K(C)}$, a slow Ca^{2+}-dependent afterhyperpolarization (AHP) conductance $g_{K(AHP)}$, and a transient inactivating K^+ conductance $g_{K(A)}$. These conductances were distributed nonuniformly over the membrane as in Traub et al. (2000). R_m was 100 kΩ/cm^2 over the soma/dendritic membrane. Inhibitory interneurons were modeled like those in Traub and Miles (1995) but excitability of dendrites was reduced by multiplying g_{Na} and $g_{K(DR)}$ by 0.1. All of the interneurons had identical

intrinsic properties but were distinguished only by connectivity pattern.

SYNAPTIC AND GAP-JUNCTIONAL INTERACTIONS. Each pyramidal cell received input from 30 other pyramidal cells and 80 interneurons (20 of each sort). Each interneuron received excitatory synaptic input from 150 pyramidal cells and inhibitory input from 60 interneurons (20 basket cells, 20 olm cells, 20 bistratified cells). Basket cells contacted the soma and most proximal dendrites of pyramidal cells and interneuron dendrites. Axo-axonic cells contacted only pyramidal cells, specifically their axon initial segment. Bistratified cells contacted basilar and midapical dendrites of pyramidal cells and all soma/dendritic compartments of interneurons and olm cells contacted even further distal apical dendrites of pyramidal cells and the same interneuronal dendrites as bistratified cells. Only α-amino-3-hydroxy-5-methyl-4-isoxazolepropionic acid (AMPA)– and γ-aminobutyric acid type A ($GABA_A$)–receptor-mediated synaptic interactions were simulated. AMPA synaptic contacts were made onto proximal basal dendrites of pyramidal cells and onto proximal dendrites of inhibitory interneurons. Unitary excitatory conductances were simulated by alpha functions of the form $c_e te^{-t/\tau}$ with $\tau = 2$ ms for pyramidal–pyramidal synapses and $\tau = 1$ ms for synapses onto interneurons. c_e ranged from $c_e = 0$ nS to $c_e = 5.4$ nS in different simulations for pyramidal cells, $c_e = 0.7$ nS for interneurons. Inhibitory conductances consisted of a step rise followed by an exponential decay: $c_i e^{-t/\tau}$, $\tau = 1$ ms for synapses made by basket cells and axo-axonic cells, $\tau = 8$ ms for synapses made by bistratified cells and olm cells. The parameter c_i was chosen as follows: $c_i = 1.0$ nS for synaptic connections from axo-axonic cells onto pyramidal cells, from bistratified cells to pyramidal cells' basal dedrites, and from basket cells onto (all types of) interneurons. $c_i = 1.5$ nS for synapses from basket cells and olm cells onto pyramidal cells and $c_i = 2.0$ nS for synaptic connections from bistratified cells to pyramidal cells' apical dendrites. For synaptic contacts from bistratified cells or olm cells onto interneurons, $c_i = 0.2$ nS. For EPSPs, reversal potential was 60 mV positive to the resting potential; for IPSPs, it was 15 mV negative to the resting potential. The condition for eliciting a postsynaptic conductance was that the membrane potential in the most distal axonal segment of the presynaptic cell be depolarized by 70 mV from rest and that there was no spike during the last 4 ms.

In addition to chemical synapses we also simulated electrical synaptic interactions. Gap junctions were modeled between the axons of pyramidal cells [fourth axonal compartment of the respective cells—modeled exactly as that in Traub et al. (2000)] and between proximal dendrites of interneurons. Unitary conductance between pyramidal cell axons was 4.2 nS; unitary conductance between interneuron dendrites was 1.84 nS. Noise was present in the system in the form of ectopic spikes generated in the most distal axonal segment. Ectopic spike rate was on average two per second per pyramidal cell axon and one per 5 s per interneuronal axon. The action of DHPG in the bath was modeled with chronically reduced AHP conductances, $g_{K(AHP)}$, and with small tonic input currents to pyramidal cells and interneurons. The addition of 5-HT to the bath already containing DHPG was modeled by increasing the excitability, here by increasing the tonic drive to pyramidal cells by about 2 mV.

Input "from area CA3": 83% (5/6) of the vertical interneurons and 10% of the pyramidal cells received a rhythmic 40-Hz input "from area CA3," modeled as EPSCs onto their proximal dendrites. $c_{in} te^{-t/\tau}$ with $\tau = 2$ ms. $c_{max} = c_{in}\tau/e = 1.5$ nS for pyramidal cells; $c_{max} = c_{in}\tau/e = 3.6$ nS for interneurons. Horizontal interneurons, like those in the real hippocampus, did not receive any rhythmic input "from area CA3." Pyramidal cell axons conducted at 0.5 mm/ms; interneuron axons conducted at 0.2 mm/ms. Rhythmic input arrived across the pyramidal cell and interneuron arrays with a 0.5 mm/ms conduction delay, i.e., it arrived at one end 3.84 ms later than at the other end.

DATA ANALYSIS AND COMPUTING ISSUES. Code was written in Fortran augmented with parallel instructions to run on an e1350 Linux Cluster. A typical 3.5-s simulation took about 6 h on six nodes (12 processors) of the 82-node cluster. (For further details on the code, contact andrea.bibbig@downstate.edu.) The database consists of >900 preliminary simulations followed by 60 further simulations performed once the basic parameter set had been chosen. Power spectra were constructed for the last 3.4 s out of 3.5 s per run using a fast Fourier transform (FFT) algorithm. Spike-timing histograms were constructed from firing times of 96 neurons of the respective population, i.e., 96 pyramidal cells or all the 96 basket or olm cells. The spike timing for Fig. 6 was triggered relative to the start of each gamma or beta beat, respectively.

RESULTS

Serotonin-induced CA1 beta rhythms

Bath application of DHPG (20 μM) generated a persistent population gamma rhythm in area CA1 ($n = 35$). Peak frequency, recorded in stratum pyramidale, was 33 (30–34) Hz and peak power was 162 (43–209) μV^2. The oscillation recorded in area CA1 was projected from area CA3. Surgical separation of area CA3 from area CA1 abolished all gamma activity in area CA1 (data not shown; Fisahn et al. 1998). In this control condition (DHPG-induced gamma oscillation) multiple simultaneous extracellular recordings revealed activity only in the gamma band in CA3 strata pyramidale and radiatum and CA1 stratum radiatum (Fig. 1). However, in CA1 stratum pyramidale a small, additional peak in the spectra was seen at 20 (16–22) Hz in 10/35 slices [median power 43.7 (15.0–65.0) μV^2].

Bath application of 5-HT (20 μM) significantly enhanced this beta-frequency spectral peak to 98.0 (41.9–169.3) μV^2 ($P < 0.001$, $n = 35$) in CA1 stratum pyramidale (Fig. 1). The residual gamma-frequency activity seen in area CA1 after 5-HT application was slightly but significantly shifted in frequency from 33 to 36 Hz ($P < 0.005$, $n = 35$) and significantly reduced in power ($P < 0.05$). No change in CA3 spectral content was seen ($P > 0.05$, $n = 35$, Fig. 1). Again, separation of area CA3 from area CA1 abolished all CA1 rhythmic activity. To further test whether the continued CA3 gamma-frequency input was essential for generating this CA1 beta rhythm we recorded from CA1 minislices. At a higher concentration of DHPG (100 μM) CA1 minislices showed a field potential oscillation with a faster frequency than that in the intact slice (45 $\pm$ 1 Hz compared with 33 Hz when driven by CA3, $P < 0.05$, $n = 11$). However, bath application of 5-HT (20 μM) did not generate any beta-frequency rhythm in any minislice tested (Fig. 1*C*). To test whether the generation of beta-frequency oscillations was caused by a general increase in CA1 excitability we pressure-ejected small volumes of ACSF containing 20 mM potassium ions onto stratum pyramidale midway along area CA1. A transient depression, followed by elevation in peak power, was seen but no significant change in frequency of field oscillation was seen (control frequency 36 $\pm$ 1 Hz, after potassium ion concentration increase 36 $\pm$ 1 Hz, $n = 5$, $P > 0.5$, Fig. 1*D*). To test whether the effect was mediated by general excitability increases caused by 5-HT we used the 5-HT2A/C receptor agonist 1-(2,5-dimethoxy-4-iodophenyl)-2-aminopropane (DOI, 20 μM) (Lee et al. 1999; Luttgen et al. 2004). DOI failed to cause a significant change in peak field oscillation frequency in area CA1 in all slices tested ($n = 5$, $P > 0.5$, Fig. 1*E*). Because neither general increases in

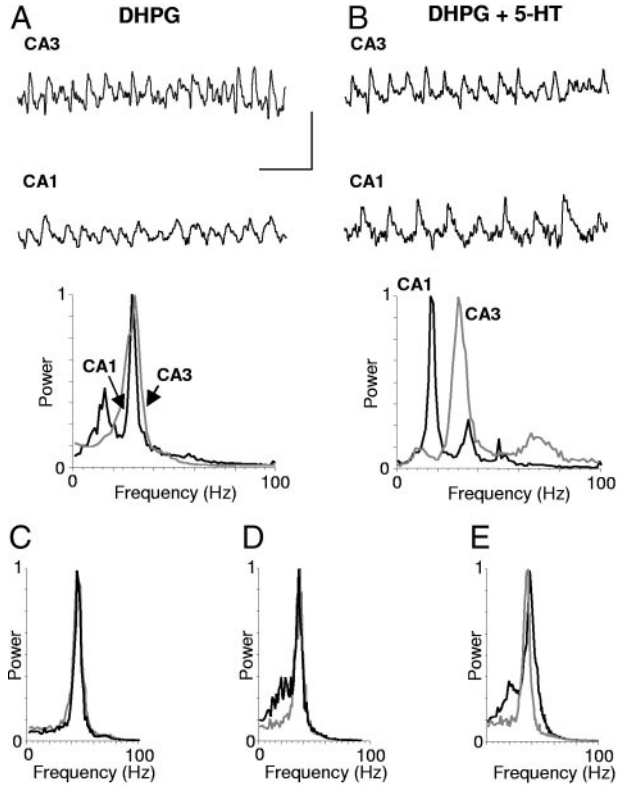

FIG. 1. 5-Hydroxytryptamine (5-HT) transforms hippocampal population gamma into a predominantly beta rhythm in area CA1 only. *A*: metabotropic glutamate receptor activation generates a population gamma rhythm in areas CA3 and CA1. Example traces show field potential recordings from stratum pyramidale in each area. Pooled spectra show frequency components of the field data ($n = 5$, 60-s epochs). Data are normalized to the peak power in each area. *B*: bath application of 5-HT (20 μM) does not change the pattern of population gamma rhythm generated in area CA3 but transforms the CA1 rhythm into a predominantly beta-frequency oscillation. Example traces are field potentials from stratum pyramidale in each area. Pooled spectra from 60-s epochs from 5 representative slices show the clear frequency separation between each area generated by 5-HT. Scale bars: 0.2 mV, 100 ms. *C*: lack of effect of 5-HT on gamma rhythms in CA1 minislices. Data show pooled power spectra ($n = 5$) from CA1 stratum pyramidale in (*S*)-3,5-dihydroxyphenylglycine (DHPG, gray line) and DHPG + 5-HT (black line), normalized to peak power. *D*: lack of significant effect of elevated extracellular potassium on gamma-frequency rhythms in area CA1. Artificial cerebrospinal fluid (ACSF) containing 20 mM potassium ions was pressure ejected onto area CA1 stratum pyramidale. Data show power spectra ($n = 5$, 60-s epochs, normalized to peak power) taken before (gray line) and after (black line) potassium elevation. *E*: lack of significant effect of the 5-HT2A/C agonist 1-(2,5-dimethoxy-4-iodophenyl)-2-aminopropane (DOI, 20 μM) on CA1 gamma frequency. Data shown as pooled power spectra ($n = 5$) before (gray line) and after (black line) bath application of DOI.

excitability nor selective 5-HT2A/C-mediated excitation caused the transition we examined in more detail the behavior of principal cells and interneurons.

The role of CA1 principal cell outputs

The generation of a beta-frequency population oscillation was accompanied by an increase in mean firing rates of CA1 pyramidal cells. During DHPG-induced gamma rhythms mean spike rates were 0 (zero to two) spike/s. This significantly increased to five (three to nine) spikes/s during beta rhythms seen during application of 5-HT ($P < 0.05$, $n = 11$, Fig. 2*A*). The power of CA1 field beta rhythms was positively correlated with the firing rate of CA1 principal cells ($R^2 = 0.675$, Fig. 2*A*). 5-HT also caused a significant, but modest depolarization (-62 ± 1 to -58 ± 1 mV, $P < 0.05$, $n = 11$) but no significant change in input resistance (56 ± 3 vs. 62 ± 4 MΩ, $P > 0.05$, $n = 11$). The depolarization in mean membrane potential was accompanied by an increase in mean EPSP amplitudes recorded at -70 mV in CA1 pyramidal cells (from 2.1 ± 0.1 to 4.1 ± 0.1 mV, $P < 0.001$, $n = 10$, Fig. 2*A*). To further analyze the relationship between firing rate of CA1 pyramidal cells and beta power we constructed a realistic model of area CA1 made to oscillate by a fixed 40-Hz frequency of concurrent inputs to model interneurons with dendrites extending into stratum radiatum and to principal cell apical dendrites to mimic a constant gamma-frequency drive from area CA3. The ratio of excitatory drive to principal cells and interneurons was 0.42. Using this model we varied only the baseline firing rate of principal cells by changing their tonic drive. This manipulation alone resulted in a positive correlation between firing rate and population beta power (Fig. 2*B*).

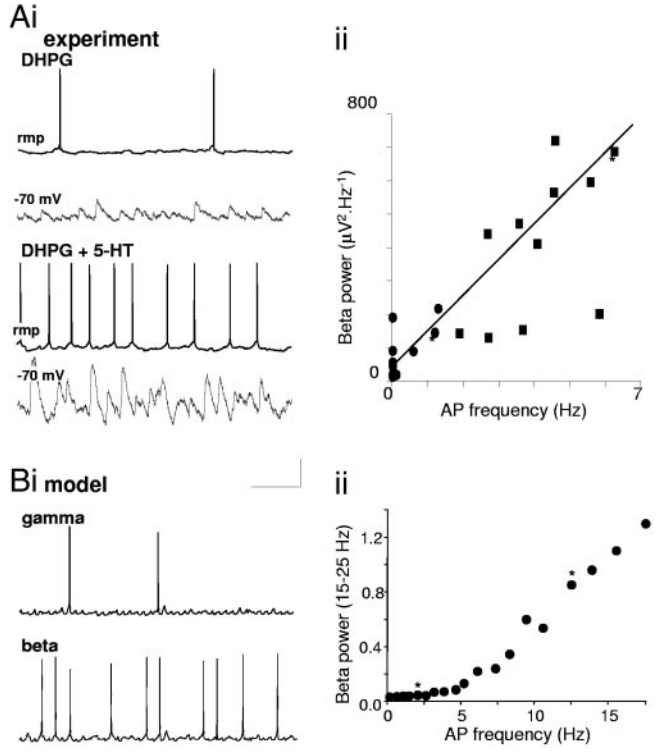

FIG. 2. Transition to beta frequency is associated with an increase in CA1 pyramidal cell spike output. *Ai*: data from experiments illustrating the change in CA1 pyramidal cell spiking on bath application of 5-HT. Example traces show somatic recordings from the same pyramid recorded during population gamma (DHPG alone) and beta (DHPG + 5-HT) rhythms. Recordings are illustrated at rmp (-62 mV in DHPG, -57 mV in DHPG + 5-HT) to show spike rate change and also at -70 mV to show the change in excitatory postsynaptic potential (EPSP) amplitude in the 2 conditions (spikes and EPSPs not recorded in parallel). *Aii*: graph shows pooled data from 11 experiments before (circles) and after (squares) 5-HT bath application, illustrating the relationship between CA1 pyramid spiking and field beta generation. Asterisks show the data points from which the 2 example traces were taken. *B*: model data showing the interrelationship between population beta-frequency rhythm and CA1 pyramidal cell output for a constant, phasic gamma input. Only the tonic drive to CA1 pyramids was changed, resulting in increased spike rates. Graph shows data from simulations in which mean spike rate was varied from 0 to 18 s^{-1}, with spike rate plotted against population beta power. Asterisks indicate the data points from which the example traces were taken. Scale bars: 20 mV (experimental and model spike data), 3 mV (EPSP data), 200 ms.

The role of CA1 interneurons

The pattern of increased principal cell outputs and recurrent excitation was previously shown to lead to beta rhythms (Whittington et al. 1997). However, in this case principal cell spike rates were very high: Action potentials were generated in each principal cell on nearly all periods of the field potential rhythm. The process causing principal cells to fire, on average, only on every other period of underlying inhibition-based gamma oscillation (missed beats) was mediated by a recovery of AHP after stimulus-induced transient metabotropic glutamate receptor activation. Because DHPG was present throughout the experiments in the present study this mechanism could not be responsible here. However, computer simulations predicted that a similar phenomenon may also occur with enhanced perisomatic inhibition onto principal cells (Bibbig et al. 2002). We therefore looked for changes in interneuron output associated with beta-frequency generation.

A large proportion of CA1 stratum radiatum and pyramidale interneurons receive excitatory input from area CA3 (Frotscher et al. 1984), whereas slow spiking stratum oriens interneurons receive mainly local excitation from CA1 pyramidal neurons (Blasco-Ibanez and Freund 1995). Thus by comparing the excitatory inputs to these two subtypes of interneuron, we were able to investigate the relative roles of feedforward (from the CA3 gamma-rhythm generator) and local feedback activation of CA1 interneurons in beta-rhythm generation.

Using the model of the CA1 network driven by a CA3 gamma-frequency input we compared the pattern of interneuron spiking in conditions that generated either a CA1 gamma output or a predominantly CA1 beta-frequency output. Four subtypes of interneuron were used in the model. Basket cells, axo-axonic cells, and bistratified cells were modeled with "vertical" dendritic arbors and could be excited by the feedforward CA3 input and feedback input from local CA1 pyramidal cells. Stratum oriens-lacunosum moleculare interneurons (olm cells) were modeled with horizontal dendrites and could be excited only by feedback input from local CA1 pyramids. Again, we used a "CA3" 40-Hz gamma feedforward drive to the model CA1 network and induced population beta rhythms in the CA1 model only by increasing pyramidal cell firing rates.

Fast-spiking interneurons receiving both local feedback excitation *and* the 40-Hz feedforward drive continued to generate action potentials on each period of the feedforward drive. However, because feedback excitation increased as a result of the increase in output from CA1 pyramids, the interneurons began to generate more spike doublets per gamma period. The incidence of spike doublets correlated with the degree of population beta rhythm produced (incidence during population gamma was 0.14 per interneuron per driven gamma period, during beta 0.33 per cell per driven gamma period). The mean interspike interval for doublet generation was 7.5 ms. Increasing the absolute refractory period of these interneurons to 20 ms, thus abolishing doublet generation, had no effect on gamma-rhythm generation but abolished the population beta rhythm (data not shown). In contrast, horizontal stratum oriens interneurons, receiving only feedback excitation, almost never generated doublets during either gamma- or beta-frequency network oscillation. Thus the model predicted that CA1 beta rhythms occurred as a consequence of doublet spiking, specifically in interneurons receiving both feedforward excitation from area CA3 and feedback excitation from local CA1 pyramids.

To test this prediction in the hippocampal slice preparation we recorded from two main types of CA1 interneuron: *1*) fast-spiking interneurons with cell bodies in stratum pyramidale and with vertically oriented dendritic arbors and *2*) slow-spiking interneurons with cell bodies in distal stratum oriens and horizontally oriented dendrites within stratum oriens (see Gloveli et al. 2005). Recordings from CA1 stratum pyramidale fast-spiking interneurons during control field gamma oscillations revealed action potential generation at a modal frequency matching the field gamma oscillation (31 ± 4 Hz, $n = 8$, Fig. 3). This modal frequency of output was unchanged after induction of beta frequency field oscillations. However, in all fast-spiking neurons tested a significant increase in the generation of multiple spikes per period of concurrent field oscillation was seen. During CA1 gamma rhythms the incidence of spike doublets was 0.05 ± 0.01 per period. During field beta rhythms the doublet incidence was 0.45 ± 0.07 per period ($P < 0.05$, $n = 8$). Spike-time histograms revealed a long interspike interval per period (7 ± 2 ms). Post hoc anatomical reconstruction revealed that all eight of these interneurons were basket cells (e.g., Fig. 3).

In contrast to the change in outputs from basket cells, slow-spiking oriens interneurons generated theta-frequency outputs during field gamma oscillations (8 ± 3 Hz, $n = 10$, Fig. 4) as previously reported (Gillies et al. 2002). No doublets at all were seen during either gamma or beta field potential rhythms but an increase in overall firing rate was seen accompanying enhanced field beta rhythms (16 ± 5 Hz, $P < 0.05$), as illustrated in spike-interval histograms (Fig. 4). Post hoc anatomical reconstruction revealed that five of these neurons were stratum oriens-lacunosum moleculare neurons and five stratum oriens neurons with both axons and dendrites arranged horizontally within stratum oriens.

This expression of a beta-frequency population rhythm and increased incidence of doublet firing in basket cells were accompanied by changes in the pattern of inhibitory postsynaptic potentials in CA1 pyramidal neurons. During control gamma-frequency field oscillations rhythmic trains of somatic IPSPs were seen at 33 ± 1 Hz ($n = 9$, Fig. 5*A*). Amplitudes showed a single modal distribution with mean 6.4 ± 0.1 mV (at membrane potential of −30 mV). During field beta oscillations the pattern of IPSPs in pyramidal cells was changed. IPSP traces (taken at membrane potential of −30 mV) showed two peaks in the power spectra. A large peak at beta frequencies (18 ± 1 Hz, $n = 9$) occurred along with a smaller peak at gamma frequencies (35 ± 1 Hz, $n = 9$, Fig. 5*A*). IPSP amplitudes were seen to vary between two modal values at 10.2 and 4.6 mV. A similar pattern of changes in IPSC inputs to model CA1 pyramids was seen in conditions generating a large population beta-frequency rhythm (Fig. 5*B*). The profile of the inhibitory input to principal cells revealed a distinct change in the temporal pattern in a comparison of behavior during field gamma and enhanced beta rhythms. During gamma rhythms, averaged IPSP profiles for consecutive periods were remarkably stereotyped (Fig. 5*C*). During enhanced field beta rhythms an alternating pattern of large and small compound IPSPs was seen. The larger compound IPSPs that

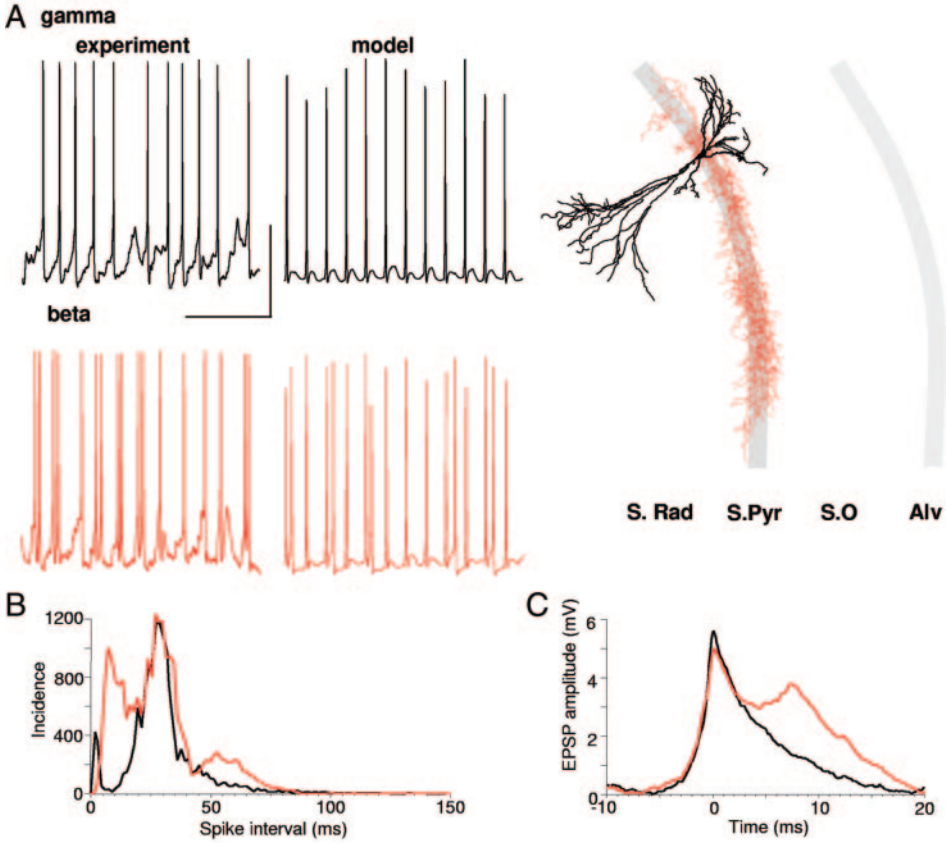

FIG. 3. Increased CA1 basket cell doublet incidence is associated with population beta rhythms. *A*: example traces showing basket cell (illustrated) spiking behavior during population gamma activity (DHPG alone) and beta activity (DHPG + 5-HT). Data from a basket cell in the model are shown on the *right* for comparison. Note the increase in doublet spikes. Scale bars: 20 mV, 100 ms. *B*: pooled interspike interval (ISI) histograms during experimental gamma (black line) and beta (red line) population rhythms illustrating both the maintenance of a gamma-frequency output from these cells during the population beta rhythm and also the appearance of doublets demonstrated by the additional peak at short ISIs. Intervals were pooled from 60-s data epochs from $n = 8$ basket cells. *C*: average EPSP profile for basket cells during population gamma (black) and beta (red) rhythms. Cells were held at −70 mV with hyperpolarizing current injection. Compound EPSPs from 10 consecutive periods were averaged, with respect to maximum peak, for each cell and this average was meaned across $n = 8$ cells using the time at EPSP maximum amplitude as the reference point. Note the lack of change in peak EPSP average amplitude but the presence of an additional, smaller component to the compound EPSP occurring with the same latency as the second spike in doublets.

occurred temporally correlated with the large positive-going deflections on the beta-frequency field potential.

Relative spike timings

To establish whether the enhancement of beta-frequency population rhythms changed the pattern of spike timings in area CA1, spike-incidence histograms were constructed with reference to the concurrently recorded field rhythm. During CA1 field gamma rhythms, basket cells were most likely to generate a single action potential 5 ms before the peak in the field potential (Fig. 6*B*). Pyramidal spiking occurred with a unimodal distribution of incidences with peak 3 ms before peak field positivity, indicating that, on average, pyramidal cells generate outputs after the local feedforward interneurons. Horizontal interneuron spikes were seen most frequently at the same time as peak firing probability for pyramidal cells (Fig. 6, *A* and *C*).

During CA1 stratum pyramidale field beta rhythms the spike-timing profiles of all three cell types changed. Basket cells continued to generate a predominantly gamma-frequency output. However, outputs timed around the peak field positivity in the beta rhythm consisted primarily of doublets (see above), whereas the spikes timed midway between adjacent field peak positivities occurred as singlets (Fig. 6*B*). Pyramidal cells demonstrated a complex, multimodal distribution of spike incidences with a much broader window of opportunity for spike generation in general. The highest probability of spiking was seen over a broad range of times around the peak positivity of the beta field potential. Within this range peaks were seen 7 and 3 ms before field positivity and 2 ms afterward. Pyramidal cells were also able to generate spikes midway between adjacent field beta peak positivities on some periods, reflecting the persistence of the feedforward gamma rhythm from area CA3 (Fig. 6*A*). Horizontal cell spiking was similar to pyramidal cell spiking during enhanced field beta rhythms. However, the peak probability of spike generation occurred midway between adjacent beta-frequency peak field positivities and multiple modal peaks occurred time-locked to the basket cell doublets, suggesting spike generation on the rebound from basket cell inhibition (Rotstein et al. 2005).

Consequences for CA3–CA1 temporal relationships

Because 5-HT induced a frequency differential between areas CA3 and CA1 we examined the consequences for the

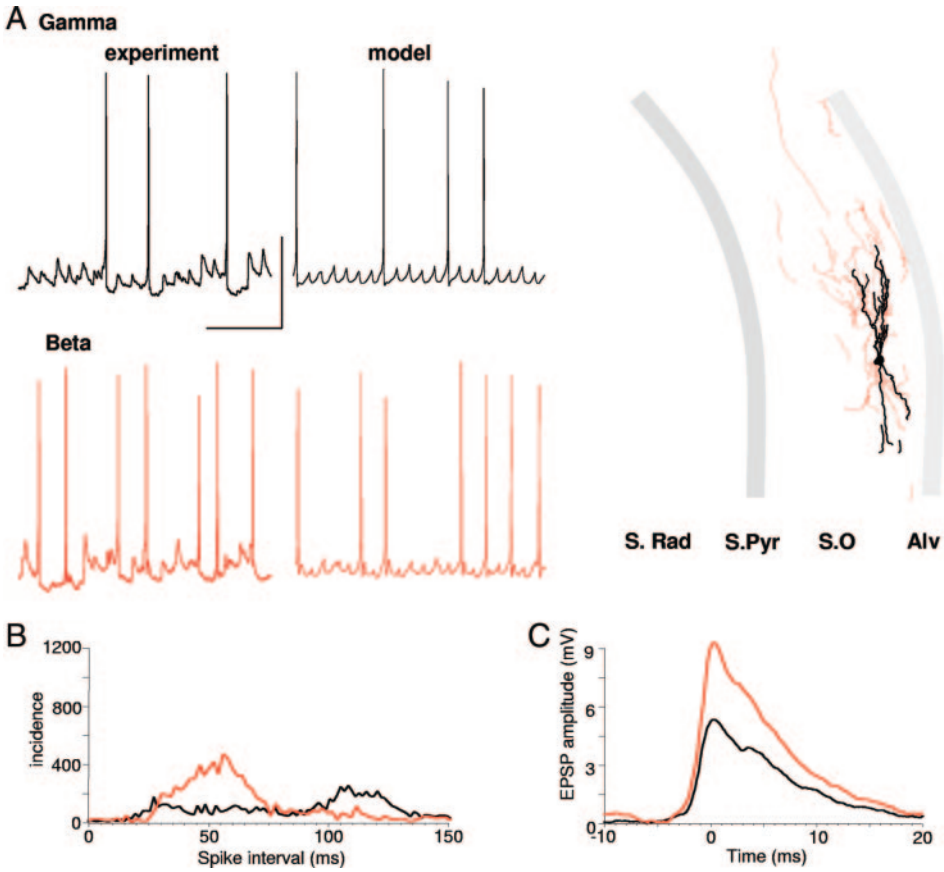

FIG. 4. Horizontal CA1 stratum oriens interneurons have increased firing rates during beta rhythms. *A*: example traces showing horizontal cell-spiking behavior during population gamma activity (DHPG alone) and beta activity (DHPG + 5-HT). Data from a stratum oriens cell in the model are shown on the *right* for comparison. Note the increase in spike rates but the absence of spike doublets. Scale bars: 20 mV, 100 ms. *B*: pooled ISI histograms during experimental gamma (black line) and beta (red line) population rhythms illustrating the decrease in ISI during the population beta rhythm. Intervals were pooled from 60-s data epochs from $n = 8$ horizontal cells. *C*: average EPSP profile for horizontal cells during population gamma (black) and beta (red) rhythms. Cells were held at −70 mV with hyperpolarizing current injection. Compound EPSPs from 10 consecutive periods were averaged, with respect to peak, for each cell and this average was meaned across $n = 8$ cells using the time at EPSP maximum amplitude as the reference point. Note the increase in peak EPSP average amplitude but the absence of the additional, smaller component to the compound EPSP seen with basket cells.

relative timing of population activity in the two subregions. When gamma rhythms alone were seen in both areas cross-correlations revealed a robust phase difference, with CA1 lagging 2 ± 1 ms ($n = 5$) behind CA3. With beta rhythms occurring in CA1 stratum pyramidale the average phase relationship changed to 1 ± 2 ms ($n = 5$, $P > 0.05$, Fig. 7*A*). Although not significant per se, this change was associated with epochs of activity in which area CA1 lead area CA3—something never previously seen when both areas expressed gamma rhythms (Fig. 7*B*). Examination of individual, nonaveraged periods of oscillation showed a broader distribution of peak CA1 field potentials with respect to fields in area CA3 (Fig. 7*C*). Examining the data in this manner further demonstrated the presence of events in which area CA1 was able to lead area CA3 and appeared to correspond with the broader distribution of CA1 pyramidal cell spike probabilities phase advanced to those seen in area CA3 (cf. Fig. 6*A*; see DISCUSSION).

DISCUSSION

Gamma-frequency oscillations in hippocampal field potentials originate in area CA3 (Chrobak et al. 2000; Fisahn et al. 1998). In the absence of external inputs to area CA1, or neuromodulatory cues, the present study demonstrates that the gamma-frequency population output from area CA3 results in a very low output from area CA1 modulated at the CA3 gamma frequency. In this state interneurons in the CA1 local circuit provide two distinct, coexistent patterns of input to principal cells: perisomatic compartments receive gamma-frequency inhibition and distal dendritic compartments receive theta-frequency inhibition (Gillies et al. 2002; Whittington and Traub 2003). However, under the influence of 5-HT, a greater degree of principal cell output was seen. The resulting population beta rhythm was associated with a change in general profile of CA3–CA1 dynamics and the convergence of output frequencies of both formerly gamma-generating perisomatic-targeting interneurons and formerly theta-generating dendritic-targeting interneurons. Neuromodulation-induced changes in frequency for rhythm-generating circuits in invertebrates (CPGs) were previously well characterized (Marder and Eisen 1984). Increases in excitability of constitutent cells is accompanied by decreases in frequency (Harris-Warrick and Marder 1991; Straub and Benjamin 2001) and involve a change in the behavior of local circuit interneurons (Yeoman et al. 1996).

Beta-frequency oscillations, in general, are associated with learning in a variety of brain regions and are enhanced, along

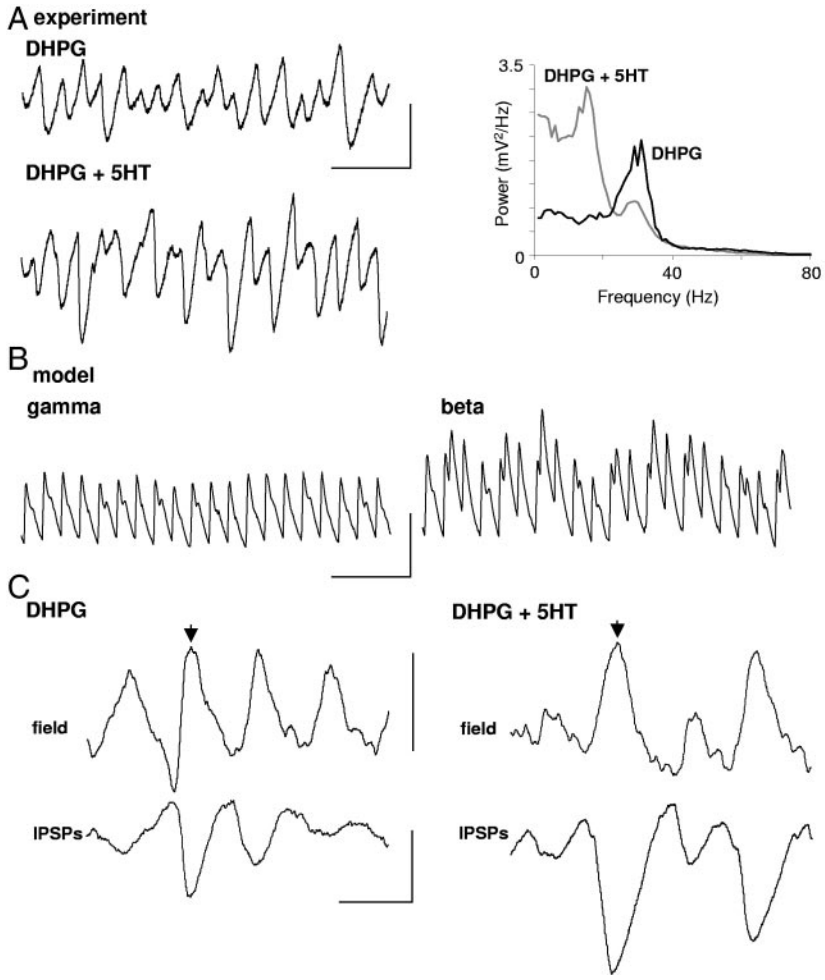

FIG. 5. Altered interneuron outputs change pyramidal cell somatic inhibition during population beta rhythms. *A*: example traces from a CA1 pyramidal neuron held at −30 mV showing the change in pattern of inhibitory postsynaptic potential (IPSP) trains before and after potentiation of the beta rhythm with 5-HT. Note the overall increase in amplitude of IPSPs and the appearance of runs of large IPSPs separated by small IPSPs. Scale bars: 5 mV, 100 ms. Graph shows pooled spectra ($n = 5$ pyramids) of 60-s epochs of IPSP trains recorded at −30 mV. Note the appearance of a prominent beta-frequency peak and the reduction in the power at gamma frequencies. *B*: example traces showing differences in pyramidal cell γ-aminobutyric acid type A ($GABA_A$) conductance between conditions generating population gamma and beta rhythms. Note the traces show conductance, whereas experimental data show potential change. Scale bars: 50 nS, 100 ms. *C*: averaged traces showing the mean temporal pattern of IPSP occurrence. *Top traces*: CA1 stratum pyramidale field recordings. *Bottom traces*: concurrently recorded IPSP trains at −30 mV. Data were taken from 10 consecutive gamma or gamma/beta periods and averaged with reference to the peak positivity in the field potential (arrows). These averages were combined into a global average ($n = 5$ cells) in each case. Note the continued presence of a partial gamma periodicity in both field and IPSP recordings during the enhanced population beta rhythm (DHPG + 5-HT). Scale bars (field): 0.1 mV (IPSP) 5 mV, 30 ms.

with certain measures of memory formation and recall by increased serotoninergic neuromodulation (Harrell and Allan 2003; Richter-Levin and Segal 1996; Sarnyai et al. 2000; Siepmann et al. 2003). Working memory of motor and auditory tasks is accompanied by an increase in functional coupling at beta frequencies (Peterson and Thaut 2002; Serrien et al. 2003). Visual short-term memory maintenance generates synchrony specifically in the beta-frequency range (Rols et al. 2001) and persistent beta-frequency oscillations were suggested to be associated with a continuous rehearsal process (Tallon-Baudry et al. 1999). In addition, beta-frequency oscillations were previously implicated in novelty detection for auditory stimuli (Haenschel et al. 2000). In rodent in vivo studies olfactory learning is associated with a twofold increase in beta power in the olfactory bulb (Ravel et al. 2003).

The modeling data demonstrated that beta rhythms may be generated solely by an increase in excitability of principal cells in areas receiving gamma-frequency input. The data obtained with serotonin certainly appear to be consistent with this prediction, with overall increases in excitability of principal cells and interneurons (using potassium pressure ejection) failing to enhance the rhythm. However, neuromodulation by 5-HT has many complex facets. We previously showed that 5-HT1A receptor activation does not generate beta rhythms (Whittington et al. 2001) and general excitation by 5-HT2 receptors also did not produce a transition to beta-frequency population rhythms (Fig. 1). Of the many other subtypes of 5-HT receptor, 5-HT3 receptors were specifically implicated in changing interneuron excitability (McMahon and Kauer 1997) and blockade of these receptors in vivo changes hippocampal theta frequency, although no effects on beta rhythms were reported (Staubli and Xu 1995). Although the present data suggest that interneuron-specific excitation may not be sufficient to generate a beta rhythm we cannot rule out a possible role for the many other serotoninergic receptor subtypes in this phenomenon. It is also interesting to note that the frequency

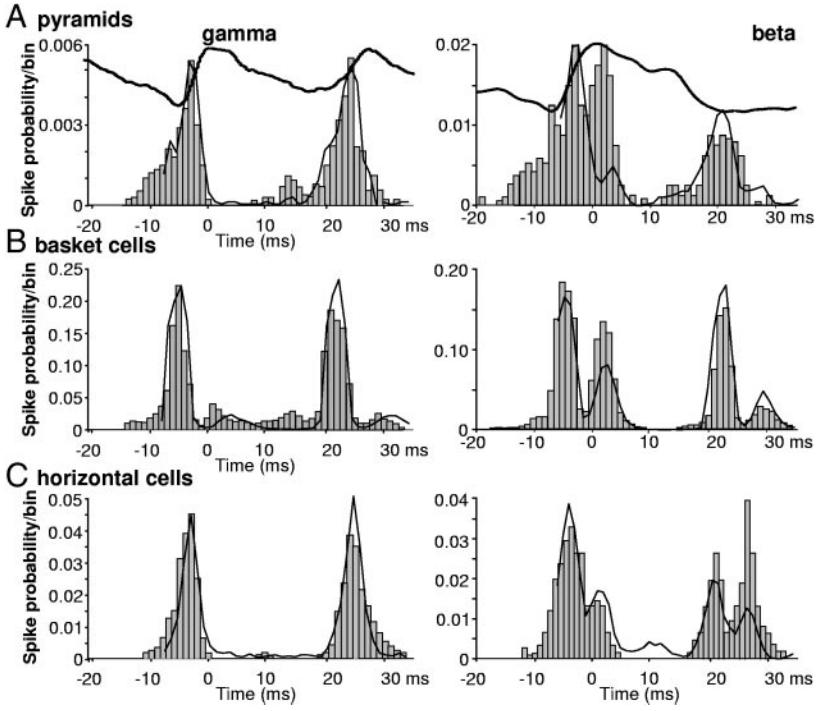

FIG. 6. Spike-timing probabilities reveal basket cell doublets and a broader temporal distribution of pyramidal cell spike timings. Spike-timing probabilities from experimental data are presented as bar graphs showing probability per 1-ms-wide bin and derived from 60-s epochs of data, one epoch per "*n*" per cell type. Spike-timing patterns calculated from model data are superimposed as line graphs and scaled to fit the peak experimental probability in 2 gamma periods or one beta period. *A*: pattern of spike timing in CA1 pyramidal cells. Mean stratum pyramidale field potentials are shown averaged relative to the peak positivity for the gamma (*left*) and enhanced beta (*right*) conditions. Note the broader distribution of spike timings around the peak field positivity and the reduced probability of spike firing one gamma period on from this reference point. *B*: during gamma rhythms basket cells fire mainly at the time of peak negativity in the stratum pyramidale field, with a smaller probability of spiking about 6 ms later corresponding to the low rate of spike doublet generation in this condition. Note that with the rhythm driven by phasic inputs from CA3, basket cell firing probability peaks slightly before pyramidal cell spiking. During beta rhythms doublet firing is dramatically increased and cells continue to generate firing at gamma frequencies. *C*: horizontal neurons show peak probabilities narrowly distributed around the peak firing for pyramidal cells. During enhanced beta rhythms horizontal cells may discharge on either of the 2 underlying gamma periods, with a bimodal distribution of spiking on the second gamma period of the field beta rhythm.

change was associated with an enhancement of EPSPs in CA1 pyramids. It is not clear at present whether this has a causal or casual relationship to the enhanced CA1 pyramidal cell output. Further work is required to establish whether this aspect of the effects of serotoninergic neuromodulation has a synaptic plasticity component.

In previous models of transition from gamma to beta rhythms in area CA1 two areas within CA1 were required to be active and plasticity of recurrent connectivity between them was essential. In addition, the enhancement in recurrent excitation had to be accompanied by an increase in pyramidal cell AHP amplitude to precipitate a beta rhythm. No such change in AHP was seen in the present study. However, enhanced GABAergic inhibitory synaptic potentials could subserve the role played by enhanced AHPs in generating beta-frequency population rhythms in area CA1 (Bibbig et al. 2002). Two possibly interdependent increases in inhibition were seen to accompany the beta rhythm here.

First basket cell outputs increased dramatically in conditions supporting beta rhythms. These cells continued to generate outputs at the gamma frequency paced by area CA3 inputs, but fired double spikes on roughly every other period (i.e., at beta frequencies). The resulting increase in somatic inhibition at beta frequencies in CA1 pyramids correlated with the increase in pyramidal cell spike rates. Basket cells may receive excitatory synaptic inputs from both feedforward inputs from area CA3 and also feedback inputs from local CA1 pyramids (Frotscher et al. 1984; Sik et al. 1995). The profile of excitatory inputs seen in these cells suggested that the enhanced output was caused entirely by the additional input received from local CA1 pyramids. Profiles consisted of two components: an initial component timed corresponding to the CA3 feedforward input during CA1 gamma rhythms, but corresponding to the local CA1 input during CA1 beta rhythms, and a second component timed to correspond best with the CA3 feedforward input during beta rhythms. Three lines of evidence suggest that the initial component of the EPSP came from local CA1 feedback connections: First, the CA1 pyramid spike-timing probabilities during beta rhythms showed a broader distribution—extending to more phase-advanced times (Fig. 6*A*). Second, cross-correlograms between CA3 and CA1 fields revealed a small additional component to the central peak, indicating the presence of epochs during which area CA1 led CA3 (Fig. 7*A*). Finally, separating area CA1 from area CA3 revealed that the fundamental network gamma frequency in the two areas was different, with area CA1 having a faster intrinsic network frequency than that of area CA3 (Fig. 1), leading to a mean period shortening in CA1 (compared with CA3) of about 8 ms (45 vs. 33 Hz), approximately the separation time between the two EPSP components seen during CA1 beta rhythms in basket cells.

This dual excitation led to temporal summation of synaptic inputs and an increase in spike doublet generation. In CA1 pyramids these spike doublets generated significantly larger

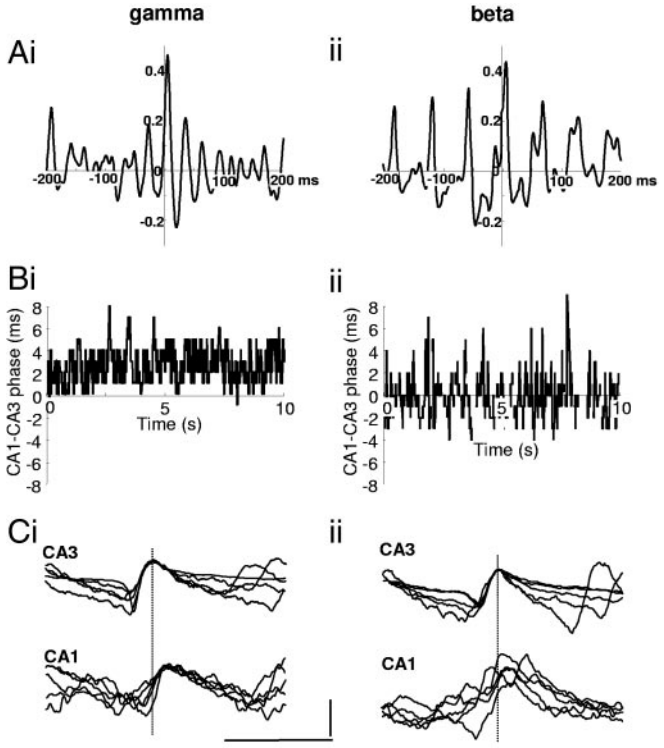

FIG. 7. CA1 beta rhythms alter the dynamic relationship between hippocampal subfields. *A*: pooled cross-correlograms (60-s epochs, $n = 5$) of CA3 stratum pyramidale vs. CA1 stratum pyramidale field potentials. *i*: average cross-correlation profile during DHPG-induced gamma rhythms. A small but robust delay between CA3 and CA1 population gamma rhythm is seen. *ii*: average cross-correlation profile during DHPG + 5-HT–induced gamma/beta rhythms. Modal central peak still shows a small delay between CA3 and CA1 but additional peaks indicate that CA1 may lead CA3 for a proportion of periods of the population rhythm. *B*: average phase plots for comparison between CA3 and CA1 stratum pyramidale field potentials. Phase lag/lead was quantified as the temporal shift in central peak of the windowed cross-correlation. Note the robust phase delay between CA3 and CA1 during gamma rhythms (*i*) is transformed into a more erratic temporal relationship with mean zero-phase delay during beta rhythms (*ii*). Brief lacunae in the data set from the beta rhythm (*Bii*) occur when the analysis program failed to detect a clear central peak. *C*: examples of CA3/CA1 field potentials during individual periods of oscillation. Traces were recorded concurrently and aligned to the peak positivity in the CA3 stratum pyramidale field. *i*: traces showing the range of temporal relationships between CA3 and CA1 during gamma rhythms. Note the robust phase lag in the *bottom CA1 traces*. *ii*: traces illustrating the range of temporal relationships between CA3 (gamma) and active CA1 periods. Note the more erratic phase relationship and the occurrence of occasional leading peaks in area CA1. Scale bars: 0.1 mV, 25 ms.

somatic IPSPs, effectively reducing the probability of CA1 pyramids to generate spikes on each consecutive CA3 gamma-frequency input (beat skipping; see INTRODUCTION). The dependency of this pattern of spiking on both feedforward and feedback inputs may also explain why area CA3 continued to generate gamma rhythms. In the DHPG model of gamma rhythms (and also the carbachol and kainate models) area CA3 constitutes the source of the gamma rhythm. No activity is seen in dentate gyrus and all activity in CA1 is abolished by separation of CA1 from CA3. Thus even in the presence of serotonin, *no* feedforward input is present in CA3 to combine with local excitation of basket cells to generate the above pattern of doublets in this subregion.

Second, an increase in the frequency of horizontal interneuronal outputs was seen. Modal output frequency doubled from theta to beta frequencies. During population gamma rhythms in area CA1 these interneurons generated a theta-frequency output (Gillies et al. 2002; Gloveli et al. 2005b). In the presence of serotonin the output increased to beta frequencies concurrently with a large increase in mean amplitude of excitatory synaptic input. Because these neurons receive the majority of their synaptic inputs from local CA1 pyramids (and not area CA3) this enhanced excitatory input appeared to be caused by the enhanced spiking rates of CA1 pyramids. Excitatory synaptic input to oriens interneurons is facilitated considerably (Ali and Thomson 1998) and long-term potentiation of these inputs was observed (Perez et al. 2001).

In vivo, serotonin receptor agonists inhibit hippocampal theta rhythms (Hirose et al. 1990) and beta-frequency outputs are seen in horizontal cells in anesthetized animals (Klausberger et al. 2003). The greater frequency of output from horizontal cells may also be related to the increase in output from basket cells. Oriens-lacunosum moleculare interneurons, in particular, possess I_h conductance (Maccaferri and McBain 1996) that may be enhanced by repetitive basket cell inhibitory potentials leading to spiking on the rebound from IPSP recovery (Rotstein et al. 2005). The present data are consistent with this mechanism because the peak probability of horizontal cell spiking was seen on the rebound from the large IPSPs temporally correlated with peak positivity in the beta-frequency population potential.

The present findings indicate that the frequencies expressed in CA1 local circuits were dependent on the degree of spiking in CA1 pyramids and that this is under control of the serotoninergic neuromodulatory system. With sparse firing, area CA1 output is strongly under the control of perisomatic inhibition driven by CA3 population gamma rhythms. However, excitatory inputs from CA3 to CA1 pyramids are gated at theta frequencies generated by distal dendrite-targeting interneurons. Thus a frequency mismatch between the gating of dendritic inputs and somatic outputs exists in these principal cells. In conditions where CA1 principal cells generate a higher degree of spiking (in this case under serotoninergic modulation), this frequency mismatch collapses. The greatest influence on pyramidal cell membrane potential of *both* perisomatic and distal dendritic targeting interneurons was at beta frequencies, permitting a greater degree of integration between excitatory input and output (somatic spiking).

In summary, nonreciprocally projected gamma rhythms influence target areas predominantly by feedforward activation of local basket cells, resulting in very low recruitment rates for target area principal cells. However, during neuromodulatory excitation, target region principal cells can be recruited. In this case the combination of feedforward and feedback excitation of interneurons serves to transfer the projected gamma rhythm into a population beta rhythm. Thus the "division of labor" proposed for interneuron subtypes in local circuit oscillating networks appears to be highly labile—being dependent on neuromodulatory cues and the degree of afferent input. Conditions may exist for all cortical networks where multiple concurrent frequencies collapse, resulting in a common mode of oscillation in which all interneuron subtypes participate.

ACKNOWLEDGMENTS

We thank R. Traub for providing code and for constant support.

GRANTS

This work was supported by The Medical Research Council, United Kingdom; The Wellcome Trust; National Institute of Neurological Disorders and Stroke of the National Institutes of Health; and Volkswagenstiftung.

REFERENCES

Ali AB, Thomson AM. Facilitating pyramid to horizontal oriens-alveus interneurone inputs: dual intracellular recordings in slices of rat hippocampus. *J Physiol* 507: 185–199, 1998.

Bibbig A, Traub RD, Whittington MA. Long-range synchronization of gamma and beta oscillations and the plasticity of excitatory and inhibitory synapses: a network model. *J Neurophysiol* 88: 1634–1654, 2002.

Blasco-Ibanez JM, Freund TF. Synaptic input of horizontal interneurons in stratum oriens of the hippocampal CA1 subfield: structural basis of feedback activation. *Eur J Neurosci* 7: 2170–2180, 1995.

Chrobak JJ, Lorincz A, Buzsáki G. Physiological patterns in the hippocampo-entorhinal cortex system. *Hippocampus* 10: 457–465, 2000.

Colino A, Halliwell JV. Differential modulation of three separate K-conductances in hippocampal CA1 neurons by serotonin. *Nature* 328: 73–77, 1987.

Csicsvari J, Jamieson B, Wise KD, Buzsáki G. Mechanisms of gamma oscillations in the hippocampus of the behaving rat. *Neuron* 37: 311–322, 2003.

Fisahn A, Pike FG, Buhl EH, Paulsen O. Cholinergic induction of network oscillations at 40 Hz in the hippocampus in vitro. *Nature* 394: 186–189, 1998.

Frotscher M, Leranth C, Lubbers K, Oertel WH. Commissural afferents innervate glutamate decarboxylase immunoreactive non-pyramidal neurons in the guinea pig hippocampus. *Neurosci Lett* 46: 137–143, 1984.

Gillies MJ, Traub RD, LeBeau FE, Davies CH, Gloveli T, Buhl EH, Whittington MA. A model of atropine-resistant theta oscillations in rat hippocampal area CA1. *J Physiol* 543: 779–793, 2002.

Gloveli T, Dugladze T, Rotstein HG, Traub RD, Monyer H, Heinemann U, Whittington MA, Kopell NJ. Orthogonal arrangement of rhythm-generating microcircuits in the hippocampus. *Proc Natl Acad Sci USA* 102: 13295–13300, 2005a.

Gloveli T, Dugladze T, Saha S, Monyer H, Heinemann U, Traub RD, Whittington MA, Buhl EH. Differential involvement of oriens/pyramidale interneurons in hippocampal network oscillations in vitro. *J Physiol* 562: 131–147, 2005b.

Haenschel C, Baldeweg T, Croft RJ, Whittington MA, Gruzelier J. Gamma and beta frequency oscillations in response to novel auditory stimuli: a comparison of human electroencephalogram (EEG) data with in vitro models. *Proc Natl Acad Sci USA* 97: 7645–7650, 2000.

Hajos N, Palhalmi J, Mann EO, Nemeth B, Paulsen O, Freund TF. Spike timing of distinct types of GABAergic interneuron during hippocampal gamma oscillations in vitro. *J Neurosci* 24: 9127–9137, 2004.

Harrell AV, Allan AM. Improvements in hippocampal-dependent learning and decremental attention in 5-HT(3) receptor overexpressing mice. *Learn Mem* 10: 410–419, 2003.

Harris KD, Csicsvari J, Hirase H, Dragoi G, Buzsáki G. Organization of cell assemblies in the hippocampus. *Nature* 424: 552–556, 2003.

Harris-Warrick RM, Marder E. Modulation of neural networks for behavior. *Annu Rev Neurosci* 14: 39–57, 1991.

Hirose A, Tsuji R, Shimizu H, Tatsuno T, Tanaka H, Kumasaka Y, Nakamura M. Inhibition by 8-hydroxy-2-(di-n-propylamino) tetralin and SM-3997, a novel anxiolytic drug, of the hippocampal rhythmical slow activity mediated by 5-hydroxytryptamine1A receptors. *Naunyn Schmiedebergs Arch Pharmacol* 341: 8–13, 1990.

Huxter J, Burgess N, O'Keefe J. Independent rate and temporal coding in hippocampal pyramidal cells. *Nature* 425: 828–832, 2003.

Klausberger T, Magill PJ, Marton LF, Roberts JD, Cobden PM, Buzsáki G, Somogyi P. Brain-state- and cell-type-specific firing of hippocampal interneurons in vivo. *Nature* 421: 844–848, 2003.

Kocsis B, Varga V, Dahan L, Sik A. Serotonergic neuron diversity: identification of raphe neurons with discharges time-locked to the hippocampal theta rhythm. *Proc Natl Acad Sci USA* 103: 1059–1064, 2006.

Kopell N, Ermentrout GB, Whittington MA, Traub RD. Gamma rhythms and beta rhythms have different synchronization properties. *Proc Natl Acad Sci USA* 97: 1867–1872, 2000.

Lee K, Dixon AK, Pinnock RD. Serotonin depolarizes hippocampal interneurones in the rat stratum oriens by interaction with 5-HT2 receptors. *Neurosci Lett* 270: 56–58, 1999.

Luttgen M, Ove Ogren S, Meister B. Chemical identity of 5-HT2A receptor immunoreactive neurons of the rat septal complex and dorsal hippocampus. *Brain Res* 1010: 156–165, 2004.

Maccaferri G, McBain CJ. The hyperpolarization-activated current (Ih) and its contribution to pacemaker activity in rat CA1 hippocampal stratum oriens-alveus interneurones. *J Physiol* 497: 119–130, 1996.

MacMahon LL, Kauer JA. Hippocampal interneurons are excited via serotonin-gated ion channels. *J Neurophysiology* 78: 2493–2502, 1997.

Mann EO, Suckling JM, Hajos N, Greenfield SA, Paulsen O. Perisomatic feedback inhibition underlies cholinergically induced fast network oscillations in the rat hippocampus in vitro. *Neuron* 45: 105–117, 2005.

Marder E, Eisen JS. Electrically coupled pacemaker neurons respond differently to same physiological inputs and neurotransmitters. *J Neurophysiol* 51: 1362–1374, 1984.

Miltner WH, Braun C, Arnold M, Witte H, Taub E. Coherence of gamma-band EEG activity as a basis for associative learning. *Nature* 397: 434–436, 1999.

Olufsen MS, Whittington MA, Camperi M, Kopell N. New roles for the gamma rhythm: population tuning and preprocessing for the beta rhythm. *J Comput Neurosci* 14: 33–54, 2003.

Perez Y, Morin F, Lacaille JC. A hebbian form of long-term potentiation dependent on mGluR1a in hippocampal inhibitory interneurons. *Proc Natl Acad Sci USA* 98: 9401–9406, 2001.

Peterson DA, Thaut MH. Delay modulates spectral correlates in the human EEG of non-verbal auditory working memory. *Neurosci Lett* 328: 17–20, 2002.

Ravel N, Chabaud P, Martin C, Gaveau V, Hugues E, Tallon-Baudry C, Bertrand O, Gervais R. Olfactory learning modifies the expression of odour-induced oscillatory responses in the gamma (60–90 Hz) and beta (15–40 Hz) bands in the rat olfactory bulb. *Eur J Neurosci* 17: 350–358, 2003.

Richter-Levin G, Segal M. Serotonin, aging and cognitive functions of the hippocampus. *Rev Neurosci* 7: 103–113, 1996.

Rodriguez E, George N, Lachaux JP, Martinerie J, Renault B, Varela FJ. Perception's shadow: long-distance synchronization of human brain activity. *Nature* 397: 430–433, 1999.

Rols G, Tallon-Baudry C, Girard P, Bertrand O, Bullier J. Cortical mapping of gamma oscillations in areas V1 and V4 of the macaque monkey. *Vis Neurosci* 18: 527–540, 2001.

Rotstein HG, Pervouchine DD, Acker CD, Gillies MJ, White JA, Buhl EH, Whittington MA, Kopell N. Slow and fast inhibition and an H-current interact to create a theta rhythm in a model of CA1 interneuron network. *J Neurophysiol* 94: 1509–1518, 2005.

Sarnyai Z, Sibille EL, Pavlides C, Fenster RJ, McEwen BS, Toth M. Impaired hippocampal-dependent learning and functional abnormalities in the hippocampus in mice lacking serotonin(1A) receptors. *Proc Natl Acad Sci USA* 97: 14731–14736, 2000.

Serrien DJ, Fisher RJ, Brown P. Transient increases of synchronized neural activity during movement preparation: influence of cognitive constraints. *Exp Brain Res* 153: 27–34, 2003.

Siepmann M, Grossmann J, Muck-Weymann M, Kirch W. Effects of sertraline on autonomic and cognitive functions in healthy volunteers. *Psychopharmacology* 168: 293–298, 2003.

Sik A, Penttonen M, Ylinen A, Buzsáki G. Hippocampal CA1 interneurons: an in vivo intracellular labeling study. *J Neurosci* 15: 6651–6665, 1995.

Staubli U, Xu FB. Effects of 5-HT3 receptor antagonism on hippocampal theta rhythm, memory and LTP induction in the freely moving rat. *J Neurosci* 15: 2445–2452, 1995.

Straub VA, Benjamin PR. Extrinsic modulation and motor pattern generation in a feeding network: a cellular study. *J Neurosci* 21: 1767–1778, 2001.

Tallon-Baudry C, Kreiter A, Bertrand O. Sustained and transient oscillatory responses in the gamma and beta bands in a visual short-term memory task in humans. *Vis Neurosci* 16: 449–459, 1999.

Traub RD, Bibbig A, Fisahn A, LeBeau FE, Whittington MA, Buhl EH. A model of gamma-frequency network oscillations induced in the rat CA3 region by carbachol in vitro. *Eur J Neurosci* 12: 4093–4106, 2000.

Traub RD, Miles R. Pyramidal cell-to-inhibitory cell spike transduction explicable by active dendritic conductances in inhibitory cell. *J Comput Neurosci* 2: 291–298, 1995.

Traub RD, Whittington MA, Buhl EH, Jefferys JG, Faulkner HJ. On the mechanism of the gamma → beta frequency shift in neuronal oscillations induced in rat hippocampal slices by tetanic stimulation. *J Neurosci* 19: 1088–1105, 1999.

Traub RD, Whittington MA, Stanford IM, Jefferys JG. A mechanism for generation of long-range synchronous fast oscillations in the cortex. *Nature* 383: 621–624, 1998.

von Stein A, Rappelsberger P, Sarnthein J, Petsche H. Synchronization between temporal and parietal cortex during multimodal object processing in man. *Cereb Cortex* 9: 137–150, 1999.

Whittington MA, Doheny HC, Traub RD, LeBeau FE, Buhl EH. Differential expression of synaptic and non-synaptic mechanisms underlying stimulus-induced gamma oscillations in vitro. *J Neurosci* 21: 1727–1738, 2001.

Whittington MA, Traub RD. Interneuron diversity series: inhibitory interneurons and network oscillations in vitro. *Trends Neurosci* 26: 676–682, 2003.

Whittington MA, Traub RD, Faulkner HJ, Stanford IM, Jefferys JG. Recurrent excitatory postsynaptic potentials induced by synchronized fast cortical oscillations. *Proc Natl Acad Sci USA* 94: 12198–12203, 1997.

Whittington MA, Traub RD, Jefferys JG. Synchronized oscillations in interneuron networks driven by metabotropic glutamate receptor activation. *Nature* 373: 612–615, 1995.

Yeoman MS, Brierley MJ, Benjamin PR. Central pattern generator interneurons are targets for the modulatory serotonergic cerebral giant cells in the feeding system of Lymnaea. *J Neurophysiol* 75: 11–25, 1996.

Zhong G, Diaz-Rios M, Harris-Warrick RM. Serotonin modulates the properties of ascending commissural interneurons in the neonatal mouse spinal cord. *Neurosci Lett* 100: 188–192, 1989.